Strojniški vestnik - Journal of Mechanical Engineering 68(2022)9, 571-582
© 2022 The Authors. CC BY 4.0 Int. Licensee: SV-JME
DOI:10.5545/sv-jme.2022.274
Original Scientific Paper
Received for review: 2022-07-08
Received revised form: 2022-09-02
Accepted for publication: 2022-09-07

Nonlinear Vibration Analysis of Functionally Graded Porous Plates Reinforced by Graphene Platelets on Nonlinear Elastic Foundations

Xiaolin Huang* – Chengzhe Wang – Jiaheng Wang – Nengguo Wei
Guilin University of Electronic Technology, School of Architecture and Transportation Engineering, China

This paper presents a nonlinear vibration analysis of functionally graded graphene platelet (GPL) reinforced plates on nonlinear elastic foundations. Uniformly or non-uniformly distributed internal pores were present in the plates. Based on the modified Halpin-Tsai micromechanics model and the extended rule of mixture, the material properties were evaluated. The governing equations, coupled with the effect of nonlinear foundations, were derived by using the higher-order plate theory and general von Kármán-type equations. A two-step perturbation technique was employed to obtain the nonlinear frequency and transient response. After the present method was verified, the effects of pores, GPLs, and elastic foundations were investigated in detail. A new finding is that the influence of the porosity coefficient on the natural frequency and dynamic response is relevant to foundation parameters. Moreover, the influence of the nonlinear foundation parameter can be negligible.

Keywords: functionally graded porous nanocomposites, graphene platelets, pores, nonlinear elastic foundation, nonlinear vibration, transient response

Highlights

- *The material properties model of functionally graded (FG) graphene platelets reinforced plates is modified.*
- *A two-step perturbation technique for the nonlinear vibration of porous plates on nonlinear elastic foundations is presented.*
- *Some interesting conclusions about the effects of pores and nonlinear elastic foundations are drawn.*

0 INTRODUCTION

Due to the excellent load-carrying capacity with stronger bonding between the matrix and carbonaceous nanofillers [1] and [2], nano graphene platelets (GPL) are now increasingly used in many engineering fields, including aerospace, automobile, and civil engineering. It is necessary to study the dynamic characteristics of GPL-reinforced composite structures.

In recent years, few results about the dynamic behaviour for functionally graded (FG) plates reinforced with GPL have been reported [3]. Song et al. [4] employed the first-order shear deformation plate theory to study the free and forced vibrations of FG multilayer GPL/polymer plates. Their results illustrated that a small amount of GPL can lead to higher natural frequency and lower dynamic response. By using the finite element method, Zhao et al. [5] studied investigated the bending and free vibration behaviours of FG trapezoidal plates. Their results also illustrated that the transient deflection was decreased by using a small number of graphene platelets. Gholami and Ansari [6] investigated the nonlinear harmonically excited vibration of FG graphene-reinforced composite plates. They found that the nonlinear buckling was increased with the rise of GPLs weight fraction. Moreover, Wu et al. [7] studied the dynamic stability of FG nanocomposite plates subjected to thermal and mechanical loads.

Recently, a novel kind of graphene-reinforced nanocomposite was made by dispersing GPL into metal foams [8] to [10]. Due to the excellent mechanical and thermal properties, the novel composite materials have attracted some attention. Kittipornchai et al. [11] proposed a micromechanical model to estimate the typical properties of FG graphene reinforced nanocomposite, in which both GPL and internal pores are uniformly dispersed within each layer. Later, the model was employed to study the dynamic behaviour of graphene-reinforced nano-composite plates [12] and [13]. In these papers, the effect of internal pores has been discussed in detail, and the results showed that both pore volume fraction and the distribution of pores can affect the dynamic characteristics of porous structures.

In practical engineering, plates are sometimes rested on elastic foundations. Thus, a suitable model is needed to evaluate foundation interaction. The simplest is the Winkler model, in which a series of springs are used to calculate the tensile and compressed forces of elastic foundations. This model was later developed into the Pasternak model, in which a shear spring is added to estimate the shear forces of

*Corr. Author's Address: Guilin University of Electronic Technology, Jinji Road 1#, Guilin, China, xlhuang@guet.edu.cn

the Winkler foundations. Thereafter, the Pasternak model has been widely used to study the static and dynamic behaviours of plates on elastic foundations [14] to [16]. To estimate the nonlinear interaction between foundations and plates, some researchers recently presented a nonlinear foundation model. For example, Nath et al. [17], Civalek [18] and Najafi et al. [19] studied the nonlinear dynamic behaviour of composite plates by using a nonlinear foundation model. Their results revealed that the nonlinear foundation parameter had a distinct influence on the dynamic characteristics.

As mentioned above, the number of studies focused on the dynamic behaviour of FG porous plates reinforced with GPL is still rather scarce. According to the authors' knowledge, no previous work has been done to study the nonlinear dynamic behaviour of FG graphene platelets reinforced porous plates on nonlinear elastic foundations. Hence, this paper attempts to study the nonlinear vibration of the plates. A modified material properties model is proposed, and the effects of internal pores and a nonlinear elastic foundation are discussed.

1 A POROUS NANO-COMPOSITE PLATE

As depicted in Fig. 1, a functionally graded graphene-reinforced porous plate (length a, width b, thickness h) on a nonlinear elastic foundation is taken into account. The origin of the coordinate system (X, Y, Z) is located at one corner of the middle plane of the plate. The Z-axis is perpendicular to the X-Y plane and points upwards. Three types of porosity distributions are considered (Fig. 2). "P-1" indicates that the largest-size pores are distributed in the middle. In contrast, "P-2" indicates that the largest-size pores are on the bottom and top surfaces. The symbol of even distribution is "P-3".

Unlike the material properties model presented by Kittipornchai et al. [11], the present model is based on the volume fraction of pores, which are assumed to be:

$$V_P(Z)=\begin{cases} e_0\cos(\pi Z/h),(P-1) \\ e_0^*\left[1-\cos(\pi Z/h)\right],(P-2). \\ 1-\alpha,(P-3) \end{cases} \quad (1)$$

In the above equation, e_0, e_0^* $(0\le e_0(e_0^*)<1$ and α denote the porosity coefficients for P−1, P−2, and P−3 distributions, respectively.

Yang's elastic modulus $E(Z)$ and shear elastic modulus $G(Z)$ of the porous plate can be expressed by using the rule of mixture:

$$E(Z)=E_0(1-V_P),$$
$$G(Z)=G_0(1-V_P), \quad (2)$$

where E_0 and G_0 are the corresponding variations of the graphene-reinforced nanocomposites without internal pores.

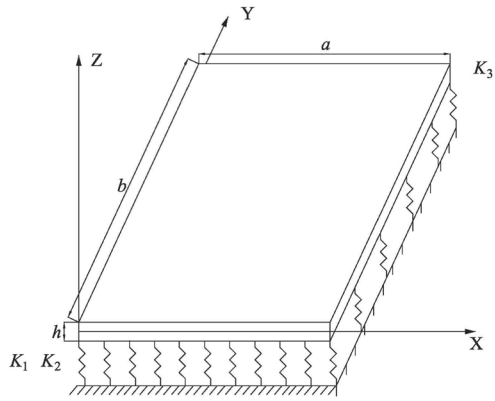

Fig. 1. *A functionally graded GPL-reinforced porous plate on a nonlinear elastic foundation*

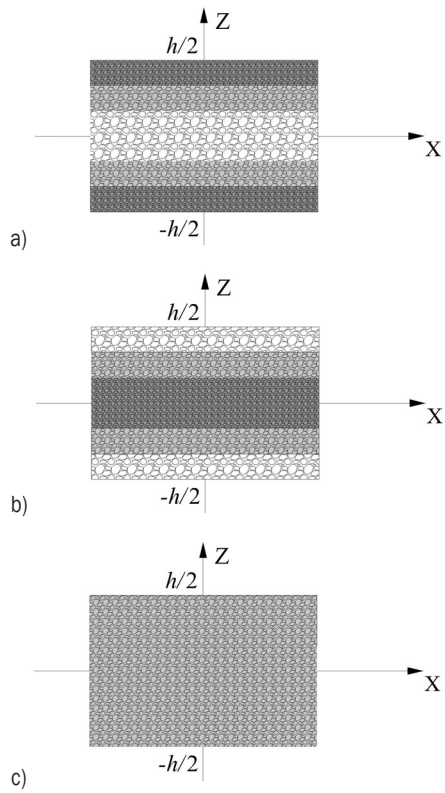

Fig. 2. *Three types of porosity distributions; a) P−1, b) P−2, and c) P−3*

Because the mass density $\rho(Z)$ cannot be calculated by using the rule of mixture [11], it is assumed to be

$$\rho(Z)=\begin{cases}\rho_0\left[1-e_1\cos\left(\pi Z/h\right)\right],(P-1)\\ \rho_0\left[1-e_1^*(1-\cos\left(\pi Z/h\right)\right],(P-2),\\ \rho_0\alpha^{'},(P-3)\end{cases} \quad (3)$$

where ρ_0 is the mass density of the nanocomposites without pores. Coefficients e_1, e_1^* and α' are the mass density coefficients for the three types of porosity distributions.

For open-cell metal foams, the relationship between Yang's elastic modulus and mass density is $\frac{E(z)}{E_0}=\left(\frac{\rho(Z)}{\rho_0}\right)^2$ [12]. Hence, the coefficients e_1, e_1^* and α' can be estimated as

$$\begin{cases}1-e_1\cos\left(\frac{\pi Z}{h}\right)=\sqrt{1-e_0\cos\left(\frac{\pi Z}{h}\right)},(P-1)\\ 1-e_1^*\left(1-\cos\left(\frac{\pi Z}{h}\right)\right)=\sqrt{1-e_0^*\left(1-\cos\left(\frac{\pi Z}{h}\right)\right)},(P-2),\\ \alpha'=\sqrt{\alpha},(P-3)\end{cases} \quad (4)$$

It is assumed that the masses of all plates with different porosity distributions are equivalent. Hence, e_0^* and α can be calculated by

$$\begin{cases}\int_{-h/2}^{h/2}\sqrt{1-e_0^*(1-\cos\left(\frac{\pi Z}{h}\right)}dZ=\int_{-h/2}^{h/2}\sqrt{1-e_0\cos\left(\frac{\pi Z}{h}\right)}dZ\\ \int_{-h/2}^{h/2}\sqrt{\alpha}=\int_{-h/2}^{h/2}\sqrt{1-e_0\cos\left(\frac{\pi Z}{h}\right)}dZ\end{cases}, \quad (5)$$

Based on the Halpin-Tsai micro-mechanical mode, the effective Young's elastic modulus E_0 can be expressed by

$$E_0=\frac{3}{8}\left(\frac{1+\xi_L\eta_L V_{GPL}}{1-\eta_L V_{GPL}}\right)E_m+\frac{5}{8}\left(\frac{1+\xi_W\eta_W V_{GPL}}{1-\eta_W V_{GPL}}\right)E_m, \quad (6)$$

where E_m and V_{GPL} are Young's elastic modulus of matrix and GPL volume fraction, respectively. The coefficients ξ_L, ξ_W, η_L and η_W are defined by

$$\eta_L=\frac{2a_{GPL}}{h_{GPL}},\quad \eta_L=\frac{2b_{GPL}}{h_{GPL}},$$
$$\eta_L=\frac{E_{GPL}/E_m-1}{E_{GPL}/E_m+\xi_L},\quad \eta_W=\frac{E_{GPL}/E_m-1}{E_{GPL}/E_m+\xi_W}, \quad (7)$$

in which E_{GPL}, a_{GPL}, b_{GPL} and h_{GPL} are Young's modulus, average length, width, and thickness of graphene platelets, respectively.

Based on the rule of mixture, Poisson's ratio v, and mass density ρ_0 can be calculated as

$$v(Z)=v_{GPL}V_{GPL}+v_m(1-V_{GPL}),$$
$$\rho_0=\rho_{GPL}V_{GPL}+\rho_m(1-V_{GPL}), \quad (8)$$

where ρ_{GPL} is the mass density of GPL, and ρ_m and v_m are the mass density and Poisson's ratio of the matrix. The shear modulus G_0 can be obtained by

$$G_0=\frac{E_0}{2\left(1+v_0\right)}. \quad (9)$$

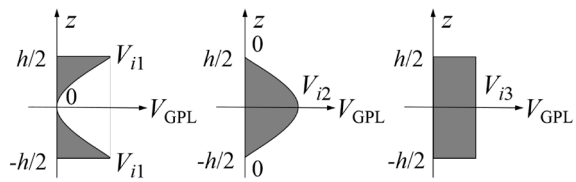

Fig. 3. *Three types of GPL dispersion patterns; a) G−1, b) G−2, and c) G−3*

As shown in Fig. 3, three types of GPL dispersion patterns (G-1, G-2, G-3) are considered. V_{GPL} is expressed as

$$V_{\mathrm{GPL}}(z)=\begin{cases}v_{i1}[1-\cos(\pi Z/h)] & (G-1)\\ v_{i1}\cos(\pi Z/h)] & (G-2),\\ v_{i3} & (G-3)\end{cases} \quad (10)$$

where v_{i1}, v_{i2} and v_{i3} are the maximum value of V_{GPL}, i ($i=1,2,3$) indicate the three types of porosity distributions. v_{i1}, v_{i2} and v_{i3} can be reckoned as follows:

$$V_{GPL}^T=\frac{W_{GPL}\rho_m}{W_{GPL}\rho_m+\rho_{GPL}-W_{GPL}\rho_{GPL}}, \quad (11)$$

$$V_{GPL}^T\int_{-h/2}^{h/2}\frac{\rho(Z)}{\rho^*}dZ=\begin{cases}\mathrm{v}_{i1}\int_{-h/2}^{h/2}\frac{\rho(Z)}{\rho^*}\left[1-\cos\left(\frac{\pi Z}{H}\right)\right]dZ\\ v_{i1}\int_{-h/2}^{h/2}\frac{\rho(Z)}{\rho^*}\cos\left(\frac{\pi Z}{H}\right)dZ\\ v_{i3}\int_{-h/2}^{h/2}\frac{\rho(Z)}{\rho^*}dZ\end{cases}, \quad (12)$$

in which V_{GPL}^T and W_{GPL} are the total volume and weight fractions of GPL, respectively.

2 FORMULATIONS

2.1 Governing Equations

As noted by Civalek [18], the effect of nonlinear plate-foundation interaction on the dynamic response of

plates on elastic foundations must not be neglected. Therefore, the following three-parameter nonlinear foundation model is adopted:

$$R_f = \bar{K}_1\bar{W} - \bar{K}_2\left(\frac{\partial^4 W}{\partial X^4} + 2\frac{\partial^4 \bar{W}}{\partial X^2\partial Y^2} + \frac{\partial^4 W}{\partial Y^4}\right) + \bar{K}_3\bar{W}^3, \quad (13)$$

where $\bar{K}_1$, $\bar{K}_2$, and $\bar{K}_3$ are Winkler, Pasternak, and nonlinear foundation parameters.

According to Reddy's higher-order thick plate theory **[20]**, the displacements of the thick composite plate are assumed to be

$$\begin{aligned}
\bar{u}_1 &= \bar{U}(X,Y,t) + Z\left[\bar{\psi}_1 - \frac{4}{3}\left(\frac{Z}{h}\right)^2\left(\bar{\psi}_1 + \frac{\partial \bar{W}}{\partial X}\right)\right],\\
\bar{u}_2 &= \bar{V}(X,Y,t) + Z\left[\bar{\psi}_y - \frac{4}{3}\left(\frac{Z}{h}\right)^2\left(\bar{\psi}_y + \frac{\partial \bar{W}}{\partial Y}\right)\right],\\
\bar{u}_3 &= \bar{W}(X,Y,t),
\end{aligned} \quad (14)$$

in which $\bar{U}$, $\bar{V}$, $\bar{W}$, $\bar{\psi}_1$ and $\bar{\psi}_2$ are the displacements and rotations of a point (X, Y) on the mid-plane.

The von Karman strains associated with the displacement field in Eq. (14) can be stated as

$$\begin{aligned}
\varepsilon_1 &= \frac{\partial \bar{U}}{\partial X} + \frac{1}{2}\left(\frac{\partial \bar{W}}{\partial X}\right)^2 + Z\frac{\partial \bar{\psi}_1}{\partial X} - \frac{4Z^3}{3h^2}\left(\frac{\partial \bar{\psi}_1}{\partial X} + \frac{\partial^2 \bar{W}}{\partial Y^2}\right),\\
\varepsilon_2 &= \frac{\partial \bar{V}}{\partial Y} + \frac{1}{2}\left(\frac{\partial \bar{W}}{\partial Y}\right)^2 + Z\frac{\partial \bar{\psi}_2}{\partial Y} - \frac{4Z^3}{3h^2}\left(\frac{\partial \bar{\Psi}_2}{\partial Y} + \frac{\partial^2 \bar{W}}{\partial Y^2}\right),\\
\varepsilon_3 &= 0, \qquad \varepsilon_4 = \bar{\psi}_2 + \frac{\partial \bar{W}}{\partial Y} - \frac{4Z^2}{h^2}\left(\bar{\psi}_2 + \frac{\partial \bar{W}}{\partial Y}\right),\\
\varepsilon_5 &= \bar{\Psi}_1 + \frac{\partial \bar{W}}{\partial X} - \frac{4Z^2}{h^2}\left(\bar{\Psi}_1 + \frac{\partial \bar{W}}{\partial X}\right),\\
\varepsilon_6 &= \frac{\partial \bar{U}}{\partial Y} + \frac{\partial \bar{V}}{\partial X} + \frac{\partial \bar{W}}{\partial X}\frac{\partial \bar{W}}{\partial Y} + Z\left(\frac{\partial \bar{\psi}_1}{\partial Y} + \frac{\partial \bar{\psi}_2}{\partial X}\right)\\
&\quad - \frac{4Z^3}{3h^2}\left(\frac{\partial \bar{\psi}_1}{\partial Y} + \frac{\partial \bar{\psi}_2}{\partial X} + 2\frac{\partial^2 \bar{W}}{\partial X\partial Y}\right).
\end{aligned} \quad (15)$$

Based on Hook's law, the relationship between stresses and strains can be expressed as

$$\begin{bmatrix}\sigma_1\\ \sigma_2\\ \sigma_6\end{bmatrix} = \begin{bmatrix}\hat{Q}_{11} & \hat{Q}_{12} & 0\\ \hat{Q}_{12} & \hat{Q}_{22} & 0\\ 0 & 0 & \hat{Q}_{66}\end{bmatrix}\begin{bmatrix}\varepsilon_1\\ \varepsilon_2\\ \varepsilon_6\end{bmatrix},$$

$$\begin{bmatrix}\sigma_4\\ \sigma_5\end{bmatrix} = \begin{bmatrix}\hat{Q}_{44} & 0\\ 0 & \hat{Q}_{55}\end{bmatrix}\begin{bmatrix}\varepsilon_4\\ \varepsilon_5\end{bmatrix}, \quad (16)$$

in which

$$\begin{aligned}
&\hat{Q}_{11} = \hat{Q}_{22} = \frac{E}{1-\nu^2}, \quad \hat{Q}_{12} = \frac{\nu E}{1-\nu^2},\\
&\hat{Q}_{16} = \hat{Q}_{26} = 0, \quad \hat{Q}_{44} = \hat{Q}_{55} = \hat{Q}_{66} = \frac{E}{2(1+\nu)}.
\end{aligned} \quad (17)$$

The in-plane forces $\bar{N}_i$, bending moment $\bar{M}_i$, higher-order bending moment $\bar{P}_i$, shear forces $\bar{Q}_i$, and higher-order shear forces $\bar{R}_i$ are

$$\begin{aligned}
\left(\bar{N}_i, \bar{M}_i, \bar{P}_i\right) &= \int_{-h/2}^{h/2}\sigma_i\left(1, Z, Z^3\right)\mathrm{d}Z, \quad (i = 1,2,6),\\
\left(\bar{Q}_2, \bar{R}_2\right) &= \int_{-h/2}^{h/2}\sigma_4\left(1, Z^2\right)\,\mathrm{d}Z,\\
\left(\bar{Q}_1, \bar{R}_1\right) &= \int_{-h/2}^{h/2}\sigma_5\left(1, Z^2\right)\,\mathrm{d}Z.
\end{aligned} \quad (18)$$

By using the Hamilton principle, the equations of motion for the plate can be derived as

$$\begin{aligned}
&\frac{\partial \bar{N}_1}{\partial X} + \frac{\partial \bar{N}_6}{\partial Y} = I_1\ddot{\bar{U}} + \bar{I}_2\ddot{\bar{\psi}}_1 - I_4\frac{4}{3h^2}\frac{\partial \ddot{\bar{W}}}{\partial X},\\
&\frac{\partial \bar{N}_6}{\partial X} + \frac{\partial \bar{N}_2}{\partial Y} = I_1\ddot{\bar{V}} + \bar{I}_2\ddot{\bar{\psi}}_2 - I_4\frac{4}{3h^2}\frac{\partial \ddot{\bar{W}}}{\partial Y},\\
&\frac{\partial \bar{Q}_1}{\partial X} + \frac{\partial \bar{Q}_2}{\partial Y} + \frac{\partial}{\partial X}\left(\bar{N}_1\frac{\partial \bar{W}}{\partial X} + \bar{N}_6\frac{\partial \bar{W}}{\partial Y}\right)\\
&\quad + \frac{\partial}{\partial Y}\left(\bar{N}_6\frac{\partial \bar{W}}{\partial X} + \bar{N}_2\frac{\partial \bar{W}}{\partial Y}\right) - \frac{4}{h^2}\left(\frac{\partial \bar{R}_1}{\partial X} + \frac{\partial \bar{R}_2}{\partial Y}\right)\\
&\quad + \frac{4}{3h^2}\left(\frac{\partial^2 P_1}{\partial X^2} + 2\frac{\partial^2 P_6}{\partial Y\partial Y} + \frac{\partial^2 P_2}{\partial Y^2}\right) + R_f\\
&= q + I_1\ddot{\bar{W}} - I_7\left(\frac{4}{3h^2}\right)^2\left(\frac{\partial^2 \ddot{\bar{W}}}{\partial X^2} + \frac{\partial^2 \ddot{\bar{W}}}{\partial Y^2}\right),\\
&\frac{\partial \bar{M}_1}{\partial X} + \frac{\partial \bar{M}_6}{\partial Y} - \bar{Q}_1 + \frac{4}{h^2}\bar{R}_1 - \frac{4}{3h^2}\left(\frac{\partial \bar{P}_1}{\partial X} + \frac{\partial \bar{P}_6}{\partial Y}\right)\\
&= \bar{I}_2\ddot{\bar{U}} + \bar{I}_3\ddot{\bar{\psi}}_x - I_5\frac{4}{3h^2}\frac{\partial \ddot{\bar{W}}}{\partial X},\\
&\frac{\partial \bar{M}_6}{\partial X} + \frac{\partial \bar{M}_1}{\partial Y} - \bar{Q}_2 + \frac{4}{h^2}\bar{R}_2 - \frac{4}{3h^2}\left(\frac{\partial \bar{P}_6}{\partial X} + \frac{\partial \bar{P}_2}{\partial Y}\right)\\
&= \bar{I}_2\ddot{\bar{V}} + \bar{I}_3\ddot{\bar{\psi}}_y - I_5\frac{4}{3h^2}\frac{\partial \ddot{\bar{W}}}{\partial Y}.
\end{aligned} \quad (19)$$

In Eq. (19), the constants I_j and $\bar{I}_j$ were given by Reddy **[20]**. The superposed dots indicate the differentiation with respect to time.

The strain compatibility equation is

$$\frac{\partial^2 \varepsilon_1^0}{\partial Y^2} + \frac{\partial^2 \varepsilon_2^0}{\partial X^2} - \frac{\partial^2 \varepsilon_6^0}{\partial X\partial Y} = \left(\frac{\partial^2 \bar{W}}{\partial X\partial Y}\right)^2 - \frac{\partial^2 \bar{W}}{\partial X^2}\frac{\partial^2 \bar{W}}{\partial Y^2}. \quad (20)$$

The in-plane forces $\bar{N}_i$ can be expressed by stress function $\bar{F}(X,Y,t)$:

$$\bar{N}_1 = \frac{\partial^2 \bar{F}}{\partial Y^2}, \quad \bar{N}_2 = \frac{\partial^2 \bar{F}}{\partial X^2}, \quad \bar{N}_6 = -\frac{\partial^2 \bar{F}}{\partial X \partial Y}. \quad (21)$$

By substituting Eqs. (18) and (21) into Eqs. (19) and (20), the governing equations of nonlinear vibration for the plate can be derived as follows:

$$\begin{aligned}
&\bar{l}_{11}(\bar{W}) - \bar{l}_{12}(\bar{\psi}_1) - \bar{l}_{13}(\bar{\psi}_2) + \bar{l}_{14}(\bar{F}) + R_f \\
&= \bar{l}(\bar{W},\bar{F}) + \bar{l}_{17}(\ddot{\bar{W}}) + I_8 \frac{\partial \ddot{\bar{\psi}}_1}{\partial X} + I_8 \frac{\partial \ddot{\bar{\psi}}_2}{\partial Y} + q, \\
&\bar{l}_{21}(\bar{F}) + \bar{l}_{22}(\bar{\psi}_1) + \bar{l}_{23}(\bar{\psi}_2) - \bar{l}_{24}(\bar{W}) = -\frac{1}{2}\bar{l}(\bar{W},\bar{W}), \\
&\bar{l}_{31}(\bar{W}) + \bar{l}_{32}(\bar{\psi}_1) - \bar{l}_{33}(\bar{\psi}_2) + \bar{l}_{34}(\bar{F}) = I_9 \frac{\partial \ddot{\bar{W}}}{\partial X} + I_{10}\ddot{\bar{\psi}}_1, \\
&\bar{l}_{41}(\bar{W}) - \bar{l}_{42}(\bar{\psi}_1) + \bar{l}_{43}(\bar{\psi}_2) + \bar{l}_{44}(\bar{F}) = I_9 \frac{\partial \ddot{\bar{W}}}{\partial Y} + I_{10}\ddot{\bar{\psi}}_2, \quad (22)
\end{aligned}$$

where the constants I_j (j=8, 9, 10), linear operators $\bar{l}_{ij}$ and nonlinear operator $\bar{l}$ were given by Shen [21] and Huang and Zheng [22].

The four edges of the plate are assumed to be simply supported. The boundary conditions are expressed as

$$\begin{aligned}
&X = 0, \quad \text{a: } \bar{W} = \bar{\psi}_1 = \bar{M}_1 = \bar{P}_1 = \bar{N}_6 = 0, \\
&Y = 0, \quad \text{b: } \bar{W} = \bar{\psi}_2 = \bar{M}_2 = \bar{P}_2 = \bar{N}_6 = 0. \quad (23)
\end{aligned}$$

2.2 Solution Procedure

To solve the nonlinear equations, Eqs. (22) and (23), we first introduce the following dimensionless parameters:

$$\begin{aligned}
&x = \frac{\pi X}{a}, y = \frac{\pi Y}{b}, z = \frac{Z}{h}, \beta = \frac{a}{b}, W = \frac{\bar{W}}{[D_{11}^* D_{22}^* A_{11}^* A_{22}^*]^{1/4}}, \\
&F = \frac{\bar{F}}{[D_{11}^* D_{22}^*]^{1/2}}, \quad (\psi_1, \psi_2) = \frac{(\bar{\psi}_1, \bar{\psi}_2)a}{\pi [D_{11}^* D_{22}^* A_{11}^* A_{22}^*]^{1/4}}, \\
&(K_1, K_2) = \frac{\left(\frac{a^4}{\pi^4}, \frac{a^2}{\pi^2}\right)}{D_{11}^*(\bar{K}_1, \bar{K}_2)}, K_3 = \frac{\bar{K}_3 a^4 \sqrt{D_{11}^* D_{22}^* A_{11}^* A_{22}^*}}{\pi^4 D_{11}^*}, \\
&\lambda_q = \frac{q a^4}{\pi^4 D_{11}^* [D_{11}^* D_{22}^* A_{11}^* A_{22}^*]^{1/4}}, \quad \tau = \frac{\pi t}{a}\sqrt{\frac{E_m}{\rho_m}}, \quad (24)
\end{aligned}$$

where the stiffness constants A_{ij}, B_{ij}, and D_{ij} are defined in the standard way [20].

The dimensionless form of the equation (22) can be rewritten as

$$\begin{aligned}
&l_{11}(W) - l_{12}(\Psi_1) - l_{13}(\Psi_2) + \gamma_1 l_{14}(F) + K_1 W - K_2 \nabla^2 W \\
&+ K_3 W^3 = \gamma_1 \beta^2 l(W,F) + l_{17}(\ddot{W}) + \gamma_2 \frac{\partial \ddot{\psi}_1}{\partial x} + \gamma_2 \beta \frac{\partial \ddot{\psi}_2}{\partial y} + \lambda_q, \\
&l_{21}(F) + \gamma_2 l_{22}(\Psi_1) + \gamma_2 l_{23}(\Psi_2) - \gamma_{24} l_{24}(W) = -\frac{1}{2}\gamma_2 \beta^2 l(W,W), \\
&l_{31}(W) + l_{32}(\psi_1) - l_{33}(\psi_2) + \gamma_1 l_{34}(F) = \gamma_4 \frac{\partial \ddot{W}}{\partial x} + \gamma_5 \ddot{\psi}_1, \quad (25)
\end{aligned}$$

where the constants $\gamma_i (i = 1, 2, ..., 5)$, the dimensionless operators l_{ij} and l can be seen in the previous work [22].

The dimensionless form of the boundary conditions in Eq. (23) are also rewritten as:

$$\begin{aligned}
&\text{x} = 0, \quad \pi: W = \psi_1 = M_1 = P_1 = N_6 = 0, \\
&y = 0, \quad \pi: W = \Psi_2 = M_2 = P_2 = N_6 = 0. \quad (26)
\end{aligned}$$

A two-step perturbation technique is employed to solve the nonlinear governing equations, Eq. (25). As the essence of this procedure, the asymptotic solution is supposed to be

$$\begin{aligned}
&W(x,y,\hat{\tau},\varepsilon) = \sum_{i=1} \varepsilon^i w_i(x,y,\hat{\tau}), \\
&F(x,y,\hat{\tau},\varepsilon) = \sum_{i=1} \varepsilon^i f_i(x,y,\hat{\tau}), \\
&\psi_x(x,y,\tilde{\tau},\varepsilon) = \sum_{i=1} \varepsilon^i \psi_{1i}(x,y,\hat{\tau}), \\
&\psi_y(x,y,\hat{\tau},\varepsilon) = \sum_{i=1} \varepsilon^i \psi_{2i}(x,y,\hat{\tau}), \\
&\lambda_q(x,y,\hat{\tau},\varepsilon) = \sum_{i=0} \varepsilon^i \lambda_i(x,y,\hat{\tau}). \quad (27)
\end{aligned}$$

In Eq. (27), the time parameter $\hat{\tau}$ ($\hat{\tau} = \varepsilon\tau$) is used to improve the perturbation procedure. Substituting Eq. (27) into Eqs. (25) and (26), then solving the perturbation equations step by step, the displacements W, ψ_x, ψ_y and stress function F can be obtained. The dimensionless transverse load λ_q can be derived as

$$\begin{aligned}
\lambda_q(x,y,\tau) &= [g_{41}\varepsilon w_1(\tau) + g_{43}\varepsilon \ddot{w}_1(\tau)]\sin mx \sin ny \\
&+ (\varepsilon w_1(\tau))^2 (g_{441}\cos 2mx + g_{442}\cos 2ny) \\
&+ g_{42}[\varepsilon w_1(\tau)]^3 (\sin mx \sin ny)^3 + o(\varepsilon^3). \quad (28)
\end{aligned}$$

In Eq. (28), it should be noted that $\hat{\tau}$ is replaced by τ. Multiplying Eq. (28) by $(\sin mx \sin ny)$ and integrating over the plate area, the following nonlinear ordinary differential equation can be obtained:

$$g_1 \frac{d^2(\varepsilon w_1)}{d\tau^2} + g_2(\varepsilon w_1) + g_3(\varepsilon w_1)^2 + g_4(\varepsilon w_1)^3 = \hat{\lambda}_q(\tau), \quad (29)$$

in which

$$\hat{\lambda}_q(\tau) = \frac{4}{\pi^2}\int_0^\pi \int_0^\pi \lambda_q(x,y,\tau)\sin mx \sin ny \, dxdy. \quad (30)$$

The nonlinear ordinary equation, Eq. (29) can be solved by using the Runge-Kutta iteration Scheme [23]. For the free vibration problem ($\lambda_q(\tau)=0$), the approximate nonlinear frequency can be derived as

$$\omega_{NL}=\left[\frac{g_{41}}{g_{43}}+\frac{9g_{42}g_{41}-10g_{44}^2}{12g_{41}g_{43}}A^2\right]^{1/2}, \qquad (31)$$

where $A=\bar{W}_{\max}/h$ is the dimensionless vibration amplitude. If A=0, the dimensionless natural frequency is $\omega_L=\sqrt{g_{41}/g_{43}}$.

3 RESULTS AND DISCUSSION

In the section, the several dimensionless parameters are used as follows:

$$k_1=\frac{\bar{K}_w a^4}{D_m},\ k_2=\frac{\bar{K}_w a^2}{D_m},\ k_3=\frac{\bar{K}_3 a^4 h^2}{D_m},$$

$$D_m=\frac{E_m h^3}{12(1-\nu_m^2)},\ \Omega=\frac{\bar{\omega}_L a^2}{h}\sqrt{\frac{\rho_m}{E_m}},\ \hat{\Omega}=\bar{\omega}_L h\sqrt{\frac{\rho_m}{E_m}}.$$

3.1 Comparison Studies

To verify the accuracy and effectiveness of the present method, two numerical examples are presented in this subsection.

Example 1. The dimensionless fundamental frequencies of GPL-reinforced porous plates resting on elastic foundations are calculated and listed in Table 1. The material properties and dimensions of GPL are E_{GPL} = 1.01 TPa, ρ_{GPL} = 1062.5 kg/m³, ν_{GPL} = 0.186, a_{GPL} = 2.5 μm, b_{GPL} = 1.5 μm, h_{GPL} = 1.5 nm. The material properties of the Matrix are E_m = 200 GPa, ρ_m = 8908 kg/m³, ν_m = 0.31.

The geometrical parameters of the plate h = 0.05 m, a = b = 1.0 m. The GPL weight fraction and porosity coefficient are W_{GPL} = 5 %, e_0 = 0.4. It can be observed that the present results are close to those given by Gao et al. [13]. The maximum error is about 2.3 %. This is because Gao et al. [13] employed the classic plate theory and differential quadrature method to calculate the fundamental frequencies, which is different from the present method.

Example 2. The dynamic response of a FG GPL reinforced plate is investigated in this example. The dispersion pattern of GPL is G−2. The plate is subjected to the explore load:

$$q(X,Y,t)=\begin{cases}P_m(1-t/t_p), 0\le t\le t_p\\ 0, \quad t<0 \text{ and } t>t_p\end{cases}, \qquad (32)$$

where the peak pulse p_m is 500 kPa and the loading time t_p is 0.01 s. The material properties of the matrix are E_m = 3.0 GPa, ρ_m = 1290 kg/m³ and ν_m = 0.34. The corresponding parameters of GPLs are E_{GPL}= 1.01 TPa, ρ_{GPL} = 1062.5 kg/m³ and ν_{GPL} = 0.186. The geometric parameters of GPLs and the plate are a = b = 0.45, h = 0.045 m, a_{GPL} = 2.5 μm, b_{GPL} = 1.5 μm and h_{GPL} = 1.5 nm. The curves of central transient deflection versus time are depicted in Fig. 4. It is found that the present results are agreement with those given by Song et al. [4].

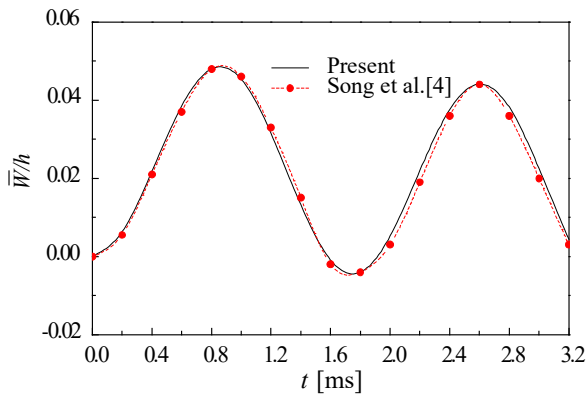

Fig. 4. *Comparison of the central transient deflection for an FG GPL-reinforced plate*

3.2 Parametric Studies

In what follows, the effects of material properties and foundation parameters are investigated in detail. The material and geometric parameters are the same as those in Example 1. Unless specially stated, the weight fraction W_{GPL} and pore coefficient e_0 are 5 % and 0.2. The dimensionless foundation parameters (k_1, k_2, k_3) are (50, 50, 50).

Table 1. *Comparison of dimensionless fundamental frequencies $\hat{\Omega}$ for GPL reinforced plates resting on Winkler-Pasternak elastic foundations*

(k_1, k_2)	Method	P−1, G−1	P−2, G−1	P−1, G−3	P−2, G−3
(100, 100)	Ref. [13]	0.0637	0.0591	0.0745	0.0696
	present	0.0652	0.0603	0.0761	0.0710
	Error [%]	2.3	2.0	2.1	2.0

Tables 2 to 4 list the fundamental natural frequencies of the plate with different GPL dispersion pattern, porosity distribution, weight fractions W_{GPL}, porosity coefficients e_0 and foundation parameters (k_1, k_2). It can be seen that the natural frequency is increased with the rising weight fraction W_{GPL} and foundation parameters (k_1, k_2). The frequency for G−1 is higher than those for G−2 and G−3. This illustrates that G−1 can strengthen the plate more effectively than the other two patterns. Also, it can be seen that the frequency for P−1 is lower than those for P−2 and P−3. The fact demonstrated that P−1 can weaken the plate more seriously. In past studies **[11]** to **[13]**, a conclusion was drawn that the natural frequency monotonously decreases with the increasing porosity coefficient. However, in the present case, the conclusion was correct only on P−2. On P−1 and P−3, the effect of the porosity coefficient

Table 2. *Dimensionless fundamental frequencies Ω for porosity distribution* P−1

GPL	e_0	$(k_1, k_2)=(0, 0)$			$(k_1, k_2)=(50, 0)$			$(k_1, k_2)=(50, 50)$		
		[wt%]			[wt%]			[wt%]		
		2.0	5.0	8.0	2.0	5.0	8.0	2.0	5.0	8.0
G−1	0.0	9.026	12.234	14.731	9.313	12.488	14.977	13.813	16.739	19.202
	0.2	8.970	12.149	14.623	9.280	12.422	14.889	14.055	16.952	19.400
	0.4	8.928	12.076	14.530	9.265	12.376	14.820	14.378	17.247	19.683
G−2	0.0	7.359	9.072	10.500	7.709	9.411	10.842	12.783	14.580	16.172
	0.2	7.311	8.997	10.404	7.687	9.363	10.773	13.056	14.848	16.440
	0.4	7.283	8.946	10.337	7.672	9.345	10.739	13.415	15.212	16.812
G−3	0.0	8.014	10.364	12.260	8.336	10.663	12.554	13.172	15.420	17.371
	0.2	7.982	10.323	12.210	8.328	10.643	12.526	13.444	15.690	17.643
	0.4	7.973	10.310	12.198	8.348	10.559	12.440	13.803	16.056	18.021

Table 3. *Dimensionless fundamental frequencies Ω for porosity distribution* P−2

GPL	e_0	$(k_1, k_2)=(0, 0)$			$(k_1, k_2)=(50, 0)$			$(k_1, k_2)=(50, 50)$		
		[wt%]			[wt%]			[wt%]		
		2.0	5.0	8.0	2.0	5.0	8.0	2.0	5.0	8.0
G−1	0.0	9.026	12.234	14.731	9.313	12.488	14.977	13.813	16.739	19.202
	0.2	8.283	11.328	13.526	8.617	11.534	13.822	13.629	16.313	18.595
	0.4	7.397	10.035	12.088	7.800	10.394	12.435	13.484	15.889	17.959
G−2	0.0	7.359	9.072	10.500	7.709	9.411	10.842	12.783	14.580	16.172
	0.2	6.775	8.382	9.719	7.180	8.774	10.112	12.765	14.486	16.017
	0.4	6.110	7.606	8.845	6.593	8.072	9.312	12.720	14.468	15.942
G−3	0.0	8.014	10.364	12.260	8.336	10.663	12.554	13.172	15.420	17.371
	0.2	7.337	9.488	11.223	7.712	9.836	11.566	13.072	15.155	16.977
	0.4	6.553	8.473	10.024	7.004	8.894	10.438	13.037	14.945	16.630

Table 4. *Dimensionless fundamental frequencies Ω for porosity distribution* P−3

GPL	e_0	$(k_1, k_2)=(0, 0)$			$(k_1, k_2)=(50, 0)$			$(k_1, k_2)=(50, 50)$		
		[wt%]			[wt%]			[wt%]		
		2.0	5.0	8.0	2.0	5.0	8.0	2.0	5.0	8.0
G−1	0.0	9.026	12.234	14.731	9.313	12.488	14.977	13.813	16.739	19.202
	0.2	9.026	12.234	14.731	9.313	12.488	14.977	13.813	16.739	19.202
	0.4	9.026	12.234	14.731	9.313	12.488	14.977	13.813	16.739	19.202
G−2	0.0	9.026	12.234	14.731	9.313	12.488	14.977	13.813	16.739	19.202
	0.2	9.026	12.234	14.731	9.313	12.488	14.977	13.813	16.739	19.202
	0.4	9.026	12.234	14.731	9.313	12.488	14.977	13.813	16.739	19.202
G−3	0.0	9.026	12.234	14.731	9.313	12.488	14.977	13.813	16.739	19.202
	0.2	8.721	11.821	14.233	9.039	12.103	14.506	13.898	16.719	19.317
	0.4	8.372	11.348	13.664	8.731	11.666	13.972	14.041	16.747	19.354

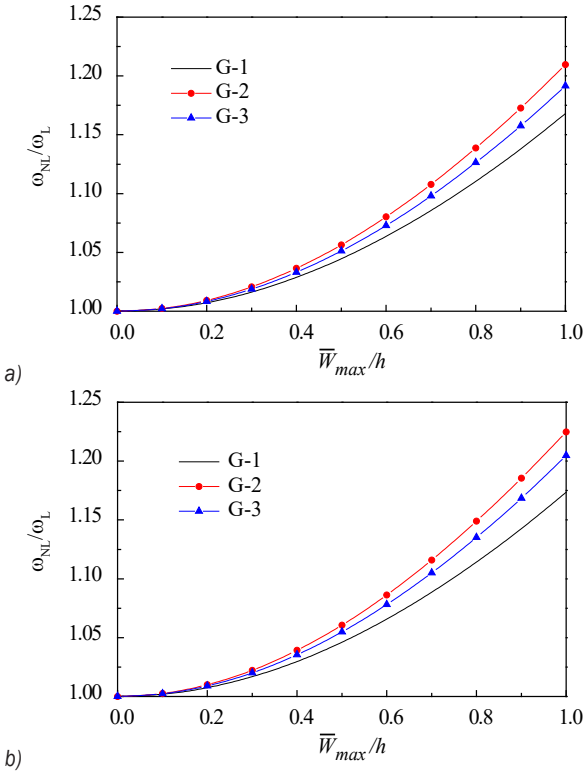

Fig. 5. *Effect of GPL dispersion pattern on the frequency ratio; a) P−1,and b) P−2*

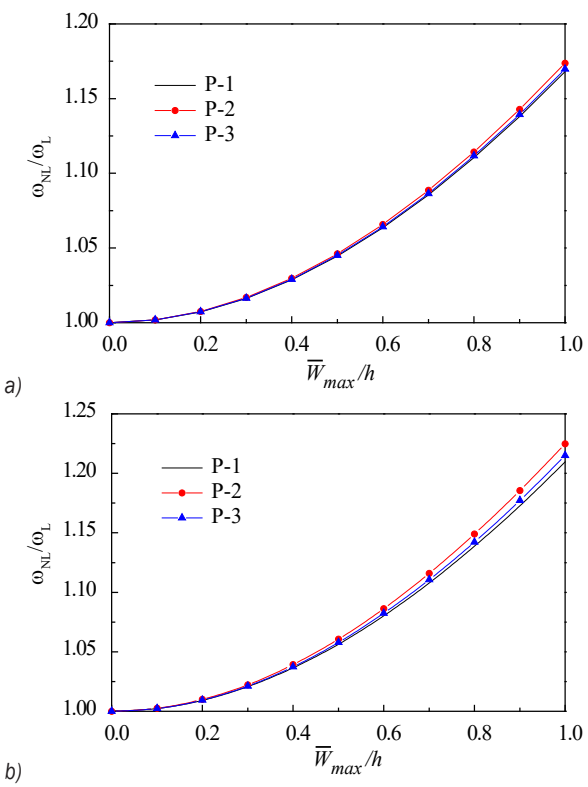

Fig. 6. *Effect of porosity distribution on the frequency ratio, a) G−1, and b) G−2*

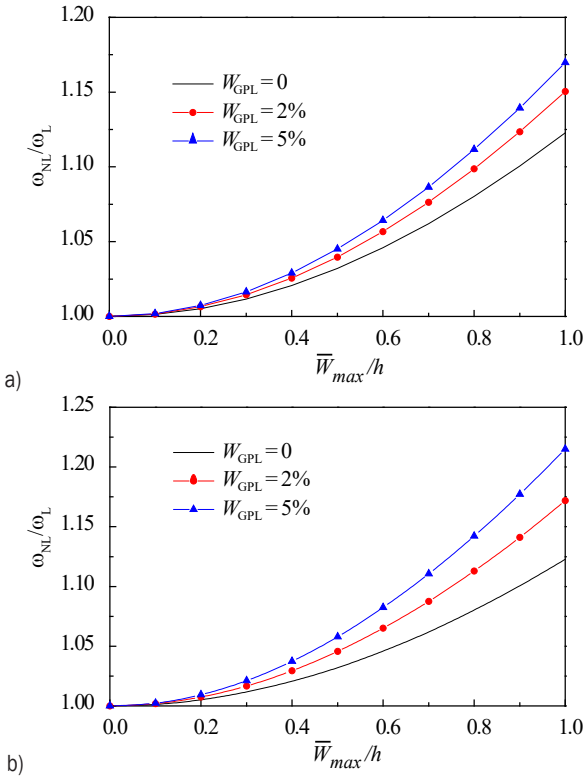

Fig. 7. *Effect of GPL weight fractions on the frequency ratio; a) G−1/P-3, and b) G−2/P−3*

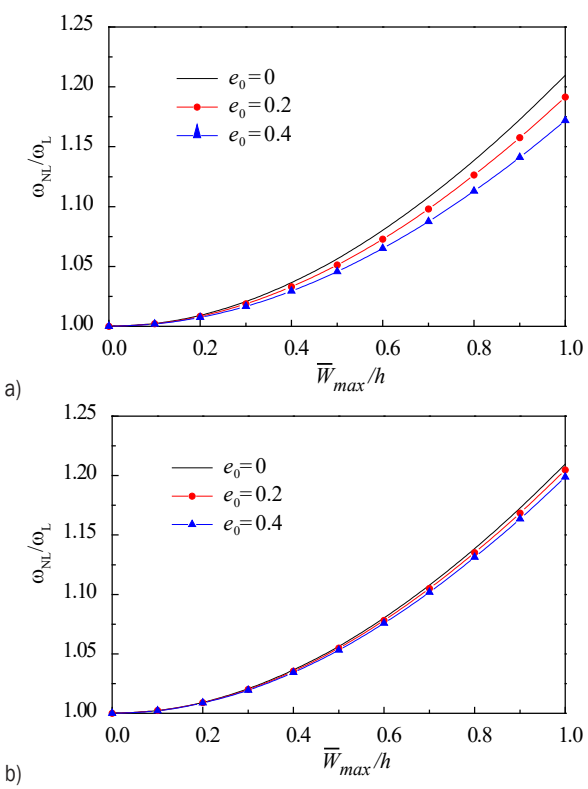

Fig. 8. *Effect of porosity coefficient on the frequency ratio; a) G−3/P−1, and b) G−3/P−2*

is relevant to the values of foundation parameters (k_1, k_2). If foundation parameters are (50, 0) or (0, 0), the natural frequency is decreased. In contrast, the natural frequency for (50, 50) is increased.

Figs. 5 to 8 reveal the influences of GPL dispersion pattern, porosity distribution, GPL weight fraction W_{GPL}, and pore coefficient e_0 on the nonlinear to linear frequency ratio ω_{NL}/ω_L. As can be observed, the frequency ratio for G−2/P−2 is higher than those for other GPL and pore distributions. The frequency ratio is decreased as pore coefficient e_0 rises but rose with the increase of GPL fraction W_{GPL}.

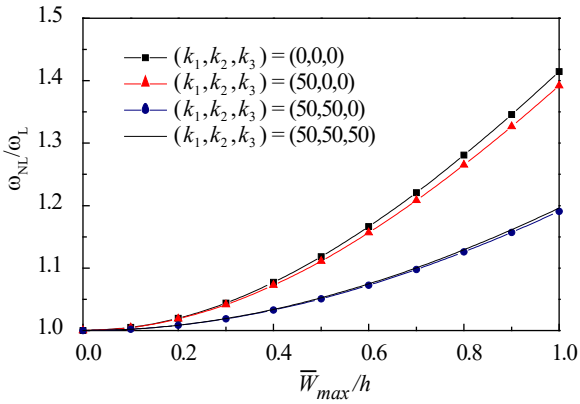

Fig. 9. Effect of elastic foundation on the frequency ratio for G−3/P−3

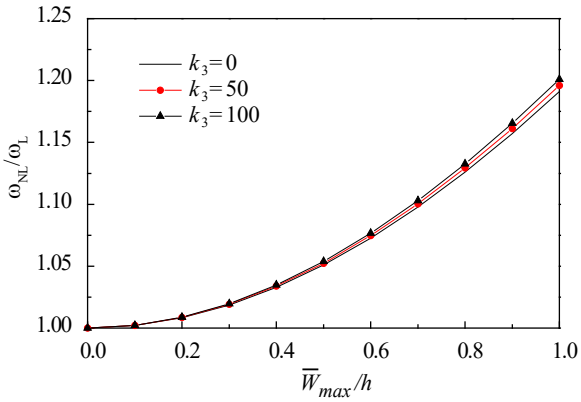

Fig. 10. *Effect foundation parameter k3 on the frequency ratio for G−3/P−3*

The effect of nonlinear elastic foundation parameters on frequency ratio is shown in Figs. 9 and 10. The two figures demonstrated that the frequency ratio reduces with the increasing parameters k_1 and k_2. However, the ratio rises as the nonlinear parameter k_3 increases.

The curves of central transient deflections and bending moments for different distributions of GPLs and pores are depicted in Figs. 11 and 12. It is found

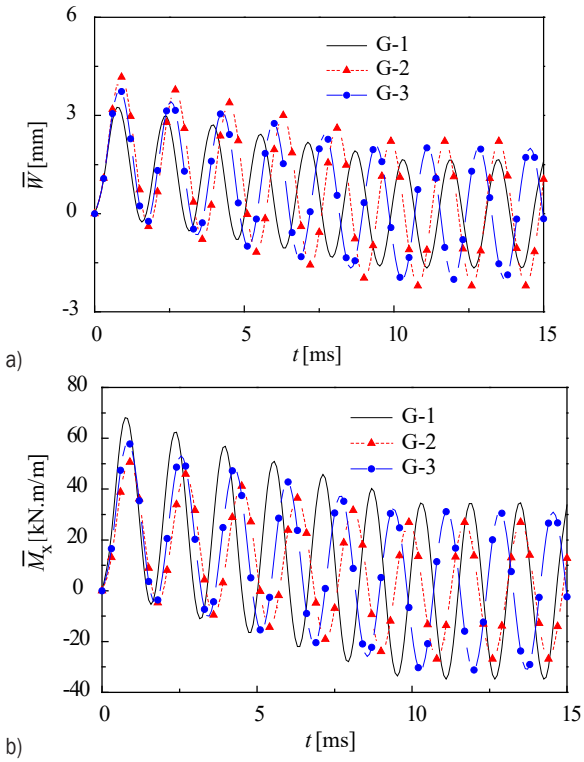

Fig. 11. *Effect of GPL dispersion patterns on the central transient responses for P−3; a) dynamic deflection, and b) dynamic bending moment*

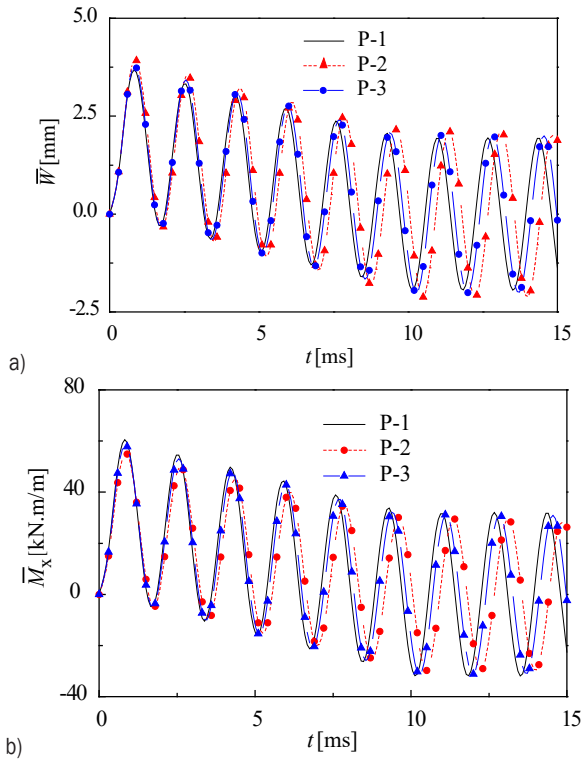

Fig. 12. *Effect of porosity distributions on the transient responses for G−3; a) dynamic deflection, and b) dynamic bending moment*

that the maximum dynamic deflection for G−2/P−2 is the largest among all patterns and distributions. In contrast, the amplitude of the dynamic bending moment for G−2/P−2 is the smallest.

The effects of GPL weight fraction W_{GPL} and pore coefficient e_0 on the transient responses is illustrated in Figs. 13 and 14. It is discerned that the rise of W_{GPL} reduces the amplitude of transient deflection, but increases the amplitude of bending moment. The maximum deflection increases by about 8 % as the porosity coefficient e_0 rises from 0.0 to 0.4. Therefore, a conclusion may be made that the effect of the porosity coefficient on the dynamic response can be negligible.

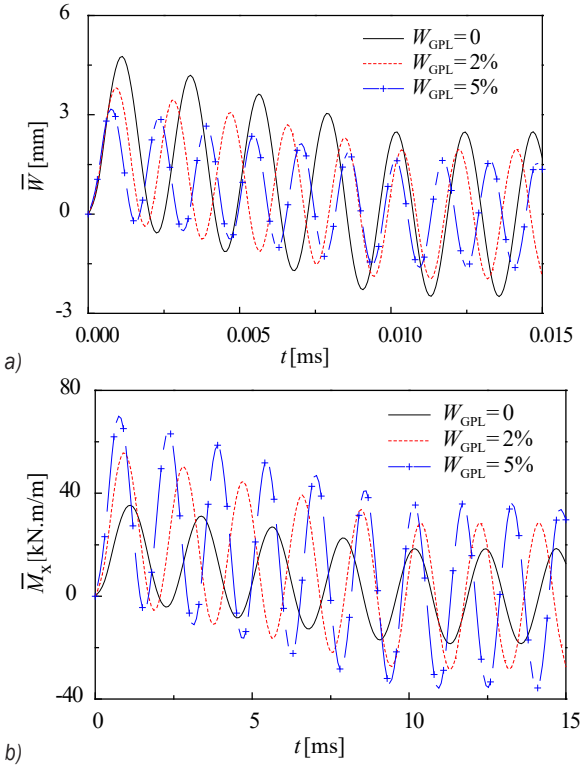

Fig. 13. *Effect of GPL weight fraction on the transient responses for P−1/G−1; a) dynamic deflection, and b) dynamic bending moment*

The effect of foundation parameters (k_1, k_2, k_3) on dynamic responses is presented in Fig. 15. As expected, Winkler and Pasternak elastic foundation parameters reduce the dynamic responses. The dynamic response for Pasternak elastic foundations (50, 50, 0) is very close to those for the nonlinear elastic foundations (50, 50, 50). Hence, a conclusion may be drawn that the effect of nonlinear foundation parameter k_3 on dynamic responses may be neglected, which is different from the statement mentioned by

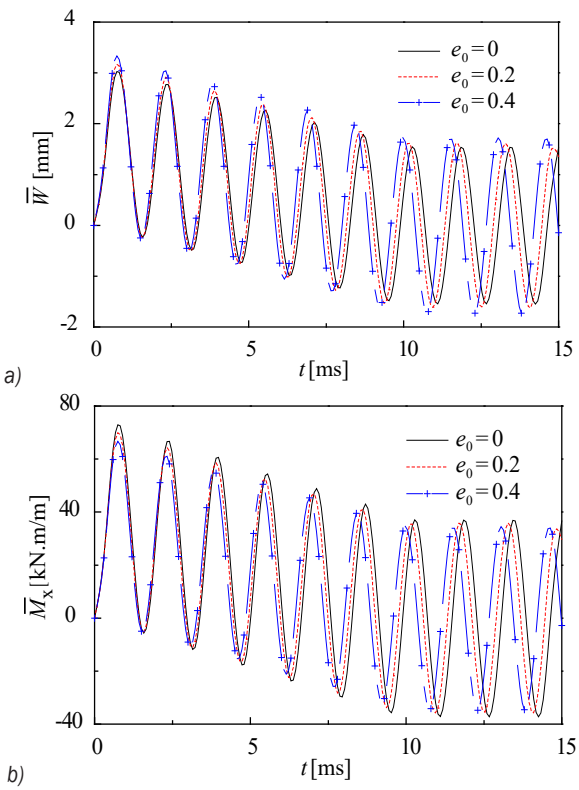

Fig. 14. *Effect of porosity coefficient on the transient responses for P−1/G−1; a) dynamic deflection, and b) dynamic bending moment*

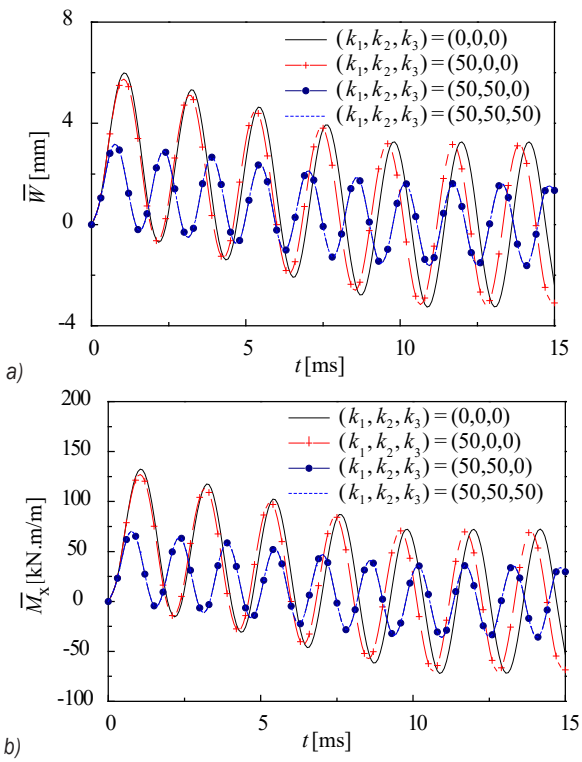

Fig. 15. *Effect of elastic foundation on the transient responses for P−1/G−1; a) dynamic deflection, and b) dynamic bending moment*

Civalek [18] and Najafi et al. [19]. They deemed that the nonlinear foundation parameter k_3 had a significant effect on the dynamic responses of laminated and FGM plates.

4 CONCLUSIONS

The present work presents a reliable and effective method to investigate the nonlinear free and forced vibrations of functionally graded GPL reinforced porous plates on nonlinear elastic foundations. The effects of internal pores, GPLs, and nonlinear elastic foundations are discussed in detail. Some interesting conclusions can be drawn from the numerical results:

1. Both GPL dispersion patterns and porosity distribution can affect the nonlinear vibrations and responses for porous plates. Furthermore, the effect of a GPL dispersion pattern is more significant than that of a porosity distribution.
2. The GPL weight fraction and foundation parameters k_1 and k_2 increase the natural frequency but decrease the nonlinear to linear frequency ratio and transient deflection.
3. The increase of porosity coefficient does not always lead to the rise of natural frequency and transient responses.
4. Nonlinear foundation parameters have insignificant effects on the nonlinear to linear frequency ratio and transient response.

5 ACKNOWLEDGEMENTS

The authors are thankful for the financial support of the National Natural Science Foundation of China [12162010] and the Natural Science Foundation of Guangxi [2021GXNSFAA 220087].

6 REFERENCES

[1] Yusufoglu, E., Avey, M. (2021). Nonlinear dynamic behavior of hyperbolic paraboloidal shells reinforced by carbon nanotubes with various distributions. *Journal of Applied and Computational Mechanics*, vol. 7, p. 913-921, **DOI:10.22055/JACM.2021.36043.2783**.

[2] Avey, M., Yusufoglu, E. (2020). On the solution of large-amplitude vibration of carbon nanotube-based double-curved shallow shells. *Mathematical Methods in the Applied Sciences*, vol. 8, p. 1-13, **DOI:10.1002/mma.6820**.

[3] Zhao, S.Y., Zhao, Z., Yang, Z.C., Ke, L.L., Kitipornchai, S., Yang, Y. (2020). Functionally graded graphene reinforced composite structures: A review. *Engineering Structures*, vol. 210, art. ID 110339, **DOI:10.1016/j.engstruct.2020.110339**.

[4] Song, M., Kittipornchai S., Yang, J., (2017). Free and forced vibrations of functionally graded polymer composite plates reinforced with graphene nanoplatelets. *Composite Structures*, vol. 159, p. 579-588, **DOI:10.1016/j.compstruct.2016.09.070**.

[5] Zhao, Z., Feng, C., Wang, Y., Yang, J. (2017). Bending and vibration of functionally graded trapezoidal nanocomposite plates reinforced with graphene nanoplatelets (GPLs). *Composite Structures*, vol. 180, p. 799-808, **DOI:10.1016/j.compstruct.2017.08.044**.

[6] Gholami R., Ansari R. (2018). Nonlinear harmonically excited vibration of third-order shear deformable functionally graded graphene platelet- reinforced composite rectangular plates. *Engineering and Structures*, vol. 156, p. 197-209, **DOI:10.1016/j.engstruct.2017.11.019**.

[7] Wu, H., Yang, J., Kittipornchai, S. (2018). Parametric instability of thermo-mechanically loaded functionally graded graphene reinforced nanaocomposite plates. *International Journal of Mechanical Science*, vol. 135, p. 431-440, **DOI:10.1016/j.ijmecsci.2017.11.039**.

[8] Bartolucci, S.F., Paras, J., Rafiee, M.A., Rafiee, J., Lee, S., Kapoor, D. (2011). Graphene-aluminum Nanocomposites. *Material Science and Engineering: A*, vol. 528, no. 27, p. 7933-7937, **DOI:10.1016/j.msea.2011.07.043**.

[9] Rashad, M., Pan, F., Tang, A., Asif, M. (2014). Effect of graphene nanoplatelets addition on mechanical properties of pure aluminum using a semi-powder method. *Progress of Natural Science: Materials International*, vol. 24, p. 101-108, **DOI:10.1016/j.pnsc.2014.03.012**.

[10] Wu, H.L, Yang, J., Kitipornchai, S. (2020). Mechanical analysis of functionally graded porous structures: A review. *International Journal of Structural Stability and Dynamics*, vol. 20, no. 13, art. ID 2041015, **DOI:10.1142/S0219455420410151**.

[11] Kittipornchai, S., Chen, D., Yang, J. (2017). Free vibration and elastic buckling of functionally graded porous beams reinforced with graphene platelets. *Material Design*, vol. 116, p. 656-665, **DOI:10.1016/j.matdes.2016.12.061**.

[12] Yang, J., Chen, D., Kittipornchai, S. (2018). Buckling and free vibration analysis of functionally graded graphene reinforced porous nanocomposite plates on Chebyshev-Ritz method. *Composite Structures*, vol. 193, p. 281-294, **DOI:10.1016/j.compstruct.2018.03.090**.

[13] Gao, K., Gao, W., Chen, D., Yang, J. (2018). Nonlinear vibration of functionally graded graphene platelets reinforced porous nanocomposite plates resting on elastic foundation. *Composite Structures*, vol. 204, p. 831-846, **DOI:10.1016/j.compstruct.2018.08.013**.

[14] Saidi, A.R., Bahaadini, R., Majidi-Mozafari, K. (2019). On vibration and stability of porous plates reinforced by graphene platelets under aerodynamic loading. *Composite Part B: Engineering*, vol. 163, p. 778-799, **DOI:10.1016/j.compositesb.2019.01.074**.

[15] Duc, N.D., Lee, J., Nguyen-Thoi, T., Thang, P.T. (2017). Static response and vibration of functionally graded carbon nanotube-reinforced composite rectangular plates resting on Winkler-Pasternak elastic foundations. *Aerospace Science and Technology*, vol. 68, p. 391-402, **DOI:10.1016/j.ast.2017.05.032**.

[16] Haciyev, V.C., Sofiyev, A.H., Kuruoglu, N. (2018). Free bending vibration analysis of thin bidirectionally exponentially graded orthortropic rectangular plates resting on two-parameter

elastic foundations. *Composite Structures*, vol. 184, p. 372-377, **DOI:10.1016/j.compstruct.2017.10.014**.

[17] Nath, Y., Prithviraju, M., Mufti, A.A. (2006). Nonlinear statics and dynamics of antisymmetric composite laminated square plates supported on nonlinear elastic subgrade. *Communication in Nonlinear Science and Numerical Simulation*, vol. 11, p. 340-354, **DOI:10.1016/j.cnsns.2004.11.003**.

[18] Civalek, Ö. (2013). Nonlinear dynamic response of laminated plates resting on nonlinear elastic foundations by the discrete singular convolution-differential quadrature coupled approaches. *Composite Part B: Engineering*, vol. 50, p. 171-179, **DOI:10.1016/j.compositesb.2013.01.027**.

[19] Najafi, F., Shojaeefard, M.H., Googarchin, H.S. (2016). Low-velocity impact response of functionally graded plates with nonlinear elastic foundation in thermal fields. *Composite Part B: Engineering*, vol. 10, p. 123-140, **DOI:10.1016/j.compositesb.2016.09.070**.

[20] Reddy, J.N. (1984). A refined nonlinear theory of plates with transverse shear deformation. *International Journal of Solids and Structures*, vol. 20, p. 881-896, **DOI:10.1016/0020-7683(84)90056-8**.

[21] Shen, H. (1997). Kármán-type equations for a higher-order shear deformation plate theory and its use in the thermal postbuckling analysis. *Applied Mathematics and Mechanics*, vol. 18, p. 1137-1152, **DOI:10.1007/BF00713716**.

[22] Huang, X.-L., Zheng, J.-J. (2003). Nonlinear vibration and dynamic response of simply supported shear deformable laminated plates on elastic foundations. *Engineering Structures*, vol. 25, p. 1107-1119, **DOI:10.1016/S0141-0296(03)00064-6**.

[23] Pearson, C.E. (1986). *Numerical Methods in Engineering & Science*. Van Nostrand Reinhold Company, New York.